Hippocampal theta rhythm and its coupling with gamma oscillations require fast inhibition onto parvalbumin-positive interneurons

Peer Wulff[a,1], Alexey A. Ponomarenko[b,1], Marlene Bartos[a], Tatiana M. Korotkova[b], Elke C. Fuchs[b], Florian Bähner[c], Martin Both[c], Adriano B. L. Tort[d,e], Nancy J. Kopell[e,2], William Wisden[a,2], and Hannah Monyer[b,2]

[a]Institute of Medical Sciences, University of Aberdeen, Aberdeen AB25 2ZD, United Kingdom; [b]Department of Clinical Neurobiology, IZN, and [c]Institute of Physiology and Pathophysiology, Im Neuenheimer Feld 326, University of Heidelberg, 69120 Heidelberg, Germany; [d]Department of Biochemistry, Federal University of Rio Grande do Sul, Porto Alegre, RS 90035, Brazil; and [e]Center for BioDynamics and Department of Mathematics, Boston University, Boston, MA 20215

Hippocampal theta (5–10 Hz) and gamma (35–85 Hz) oscillations depend on an inhibitory network of GABAergic interneurons. However, the lack of methods for direct and cell-type-specific interference with inhibition has prevented better insights that help link synaptic and cellular properties with network function. Here, we generated genetically modified mice (PV-Δγ2) in which synaptic inhibition was ablated in parvalbumin-positive (PV+) interneurons. Hippocampal local field potential and unit recordings in the CA1 area of freely behaving mice revealed that theta rhythm was strongly reduced in these mice. The characteristic coupling of theta and gamma oscillations was strongly altered in PV-Δγ2 mice more than could be accounted for by the reduction in theta rhythm only. Surprisingly, gamma oscillations were not altered. These data indicate that synaptic inhibition onto PV+ interneurons is indispensable for theta- and its coupling to gamma oscillations but not for rhythmic gamma-activity in the hippocampus. Similar alterations in rhythmic activity were obtained in a computational hippocampal network model mimicking the genetic modification, suggesting that intrahippocampal networks might contribute to these effects.

compartmental model | GABA | GABAA receptor | knockout | network synchrony

How is information coded in the brain? Action potential firing by individual neurons is certainly central but might not be sufficient. Oscillations of the extracellular field potential may provide temporal reference signals that allow efficient information processing by spiking neurons (1–5). Multiple layers of information could be encoded if the different rhythms interact. One example is the coupling of hippocampal theta and gamma oscillations during exploratory activity and paradoxical/rapid eye movement sleep (6–9). Here, the power (or amplitude) of the gamma oscillations is systematically modulated (coupled) during each theta cycle. Such cross-frequency coupling may aid the execution of cognitive functions such as working memory (10–15).

A striking feature of the hippocampal circuit is the web of inhibition provided by diverse types of local GABAergic interneurons and externally from the medial septum - diagonal band of Broca (MS) (2, 16–19). Indeed, fast synaptic inhibition shapes both theta and gamma oscillations and could also control cross-frequency coupling (6, 16, 20–22). Because local GABAergic interneuron subtypes fire with distinct phase-related patterns (2, 23–26), each subtype probably has a distinct role in orchestrating and/or responding to the rhythm.

In this article we focus on parvalbumin-positive (PV+) interneurons. In CA1, PV+ cells comprise dendrite targeting bistratified and possibly O-LM cells, and perisomatic targeting basket cells (BCs) and axo-axonic cells (2). The latter 2 types are probably important for generating the synchronous network activity. Each of the perisomatic inhibitory PV+ cells innervates >1000 pyramidal cells (27, 28) and fires phase-locked to theta and gamma oscillations

evoking rhythmic perisomatic inhibitory postsynaptic currents (IPSCs) in the pyramidal cell layer (6, 7, 9, 24, 29). Via synaptic GABAA receptors, PV+ BCs reciprocally inhibit each other and receive inhibition from the MS and other local interneurons (19, 20, 30). To investigate how GABAergic inhibition of PV+ cells contributes to the generation and coupling of theta and gamma oscillations in the hippocampus, we selectively removed fast synaptic GABAergic inhibition from these cells, using mouse transgenic methods.

Results

Selective Removal of the GABAA Receptor γ2 Subunit from PV+ Neurons. PV+ interneurons in the hippocampus express αβγ2-type GABAA receptors (31, 32). The γ2 subunit is essential to traffic and to anchor the receptor to the postsynaptic membrane and it confers full single channel conductance to the receptor (33, 34). Thus, removing the γ2 subunit impairs GABAA receptor function and removes fast synaptic inhibition (35). To investigate the role of fast synaptic inhibition of PV+ interneurons in hippocampal network activity, we selectively ablated the γ2 subunit from these cells (PV-Δγ2 mice, see *Materials and Methods* for details) and thus disconnected them from the fast inhibitory network.

Deletion of the γ2 subunit was examined by in situ hybridisation with a γ2 subunit-specific probe (36). At the level of X-ray film analysis, the hippocampus and neocortex of PV-Δγ2 mice showed a γ2 mRNA signal comparable to littermate controls. This was expected because PV+ cells are a minority in these areas. However, areas with a high number of PV+ cells, such as the inferior colliculus or cerebellum, showed a large reduction in the γ2-specific mRNA signal. No γ2 mRNA was present in the reticular thalamus of PV-Δγ2 mice, which contains only PV+ cells (Fig. S1). PV-Δγ2 mice appeared normal in the first 3 postnatal weeks, but showed reduced body weight, tremor and ataxia (probably because of the loss of the γ2 subunit in PV-expressing cells in motor areas) at P60. PV-Δγ2 mice had a normal life expectancy. General brain morphology was unaltered in PV-Δγ2 mice (Fig. S2). No difference in number (81.8 ± 4.9 vs. 80.5 ± 8.1 cells per hippocampus; p ≈ 0.8; unpaired students *t* test), distribution and morphology of hippocam-

© 2009 by The National Academy of Sciences of the USA

pal PV+ interneurons were detected between PV-$\Delta\gamma_2$ mice and littermate controls, using light microscopy. In principle, other γ subunits in the GABA$_A$ receptor gene family could substitute for the synaptic targeting function of γ_2 in PV-$\Delta\gamma_2$ mice. We thus analyzed the expression of the γ_1 and γ_3 subunit genes by in situ hybridisation but found no up-regulation of γ_1 or γ_3 subunit mRNA in brains of PV-$\Delta\gamma_2$ mice (Fig. S3).

GABA$_A$ Receptor-Mediated Synaptic Inhibition of Fast-Spiking Interneurons Is Lost in PV-$\Delta\gamma_2$ Mice. To confirm the loss of GABA$_A$ receptor-mediated synaptic transmission onto PV+ interneurons, we performed whole-cell patch-clamp recordings in acute hippocampal slice preparations from adult PV-$\Delta\gamma_2$ and control mice. IPSCs were recorded in CA1 BCs during extracellular stimulation and peak amplitude and decay time constant of IPSCs were compared with data obtained from recordings in pyramidal cells (PCs) under identical extracellular stimulation conditions (Fig. 1, see *Materials and Methods* for details).

In control mice both BCs and PCs had fast IPSCs with comparable peak amplitudes (250.3 ± 24.7 pA vs. 192.8 ± 29.9 pA; p ≈ 0.9; n = 4). The average decay time constant was approximately 2-fold faster in BCs than in PCs (BC: 4.3 ± 0.5 vs. PC: 8.05 ± 1.1 ms; p ≈ 0.021; n = 4; Fig. 1 *B* and *C*). In contrast, fast IPSCs were absent in 5 of 6 BCs in PV-$\Delta\gamma_2$ mice. Instead, currents with small peak amplitudes (25.7 ± 9.8 pA) and slow variable decay time constants (23.9 ± 5.9 ms) were seen (Fig. 1 *B–E*). These currents were blocked by bicuculline (n = 3; data not shown) and may reflect spillover of synaptically released GABA onto low-conductance extrasynaptic $\alpha\beta$ subunit-containing GABA$_A$ receptors (33). Accordingly, in PV-$\Delta\gamma_2$ mice the peak amplitude of inhibitory responses was markedly smaller in BCs than in PCs (BC 25.7 ± 9.8 pA vs. PC 215.4 ± 45.7 pA, p ≈ 0.0039, n = 6; Fig. 1 *B* and *C*) and the remaining small inhibitory component was markedly slowed down (decay time constant BCs: 23.9 ± 5.9 ms vs. PC: 10.15 ± 2.06 ms; p ≈ 0.078; n = 6). When peak amplitudes of compound IPSCs from all BCs of PV-$\Delta\gamma_2$ and littermate control mice were plotted as a function of their corresponding decay time constants, data distributed into 2 distinct groups (Fig. 1*E*). IPSCs in the first group were characterized by large peak amplitudes (> 50 pA) and fast decay time constants (< 10 ms) and included all BCs recordings from control and 1 of 6 recordings from PV-$\Delta\gamma_2$ BCs. IPSCs in the second group were characterized by a small peak amplitude (≤ 50 pA) and slow decay time constant (≥ 10 ms) and included 5 of 6 BC recordings from PV-$\Delta\gamma_2$ slices.

Theta Oscillations Are Reduced in PV-$\Delta\gamma_2$ Mice. Inhibitory control of PV+ interneurons has been suggested to be required for the generation of hippocampal theta rhythm (19, 21, 22, 37). To test this hypothesis we recorded local field potentials (LFP) and unit activity in CA1 stratum pyramidale in behaving PV-$\Delta\gamma_2$ and control mice, using wire electrodes during exploration in an open field and sleep in a home cage. Theta oscillations (5–10 Hz) were strongly reduced in PV-$\Delta\gamma_2$ mice (Fig. 2*A* and Fig. S4*B*). Power spectral density (PSD) in the theta frequency band and its harmonics were several fold reduced in PV-$\Delta\gamma_2$ mice (Fig. 2*B*). Integral PSD in the theta band was significantly different between genotypes (8 control and 8 PV-$\Delta\gamma_2$ mice, $F_{1,22}$ = 26.4, P < 0.0001, 2-way ANOVA). Concurrently LFP amplitudes were markedly reduced (0.29 ± 0.03 vs. 0.14 ± 0.03 mV, $F_{1,22}$ = 10.9, P < 0.01, ANOVA) and cycle duration was increased (Fig. 2*B*, *Upper Inset*). The leading frequency of theta oscillations was lower in PV-$\Delta\gamma_2$ mice by ≈1.5 Hz ($F_{1,22}$ = 20.7, P < 0.001, Fig. 2*B Lower Inset*). The theta rhythm was also less stable in PV-$\Delta\gamma_2$ mice. Frequency and amplitude variability of theta oscillation were elevated in the PV-$\Delta\gamma_2$ mice (amplitude variance was normalized by the mean amplitude: 0.09 ± 0.01 vs. 0.13 ± 0.01, $F_{1,22}$ = 16.2, P < 0.001; normalized frequency variance: 0.03 ± 0.01 vs. 0.07 ± 0.01 in control and PV-$\Delta\gamma_2$ mice respectively, $F_{1,22}$ = 32.2, P < 0.0001). Features of theta oscillations did not differ between
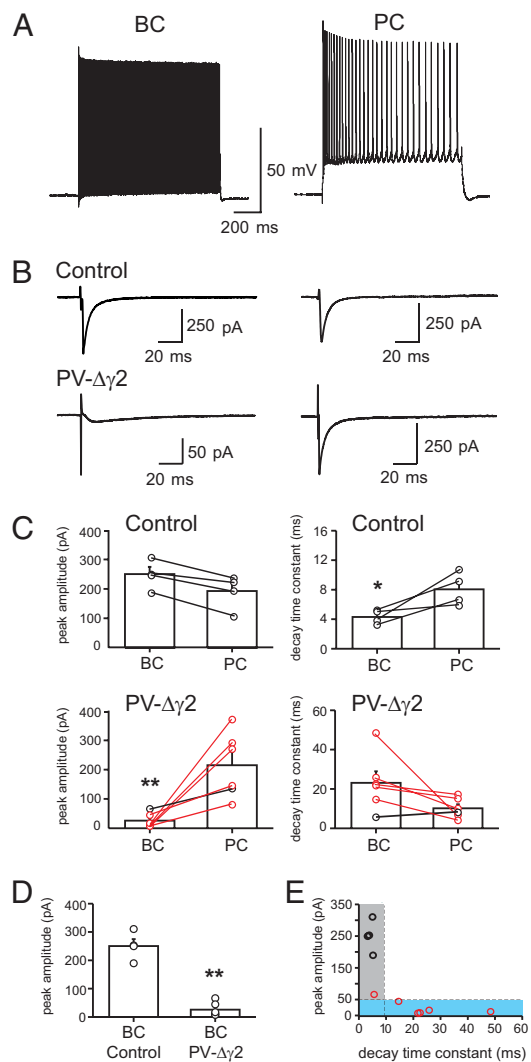

Fig. 1. Selective loss of fast synaptic inhibition onto CA1 BCs of PV-$\Delta\gamma_2$ mice. (*A*) BCs in PV-$\Delta\gamma_2$ mice show typical fast, nonaccommodating discharge when depolarized with positive current injections. PV-$\Delta\gamma_2$ PCs have a typical slow-spiking accommodating firing pattern. (*B*) Sequential recordings of compound IPSCs in BCs (left traces) and PCs (right traces) in the CA1 region of control and PV-$\Delta\gamma_2$ hippocampal slices. Traces are averages of 20–30 sweeps. Note the difference in peak amplitude and kinetics of BC and PC recordings from PV-$\Delta\gamma_2$ mice, and between BC recordings from PV-$\Delta\gamma_2$ and control mice. (*C*) Summary bar graphs of mean peak amplitude and average decay time constant of compound IPSCs. Circles connected by lines represent sequential recordings. (*D*) Comparison of mean peak amplitudes of compound IPSCs between BCs in control and PV-$\Delta\gamma_2$ mice. (*E*) Peak amplitudes of BC IPSCs from control (black circles) and PV-$\Delta\gamma_2$ mice (red circles), plotted as a function of corresponding decay time constants (n = 10). Data fell into 2 subgroups. The first group (gray area) contains IPSCs with peak amplitudes >50 pA, decay time constants <10 ms. It contains all BC recordings from control mice (n = 4) and 1 from PV-$\Delta\gamma_2$ mice. The second group (blue area) contains IPSCs with peak amplitudes ≤50 pA, decay time constants ≥10 ms and contains 5 of 6 BC recordings in PV-$\Delta\gamma_2$ mice. Bars indicate mean with SEM. *, $P \le 0.05$; **, $P \le 0.01$.

paradoxical sleep (PS) and waking in either genotype (p ≈ 0.08, ANOVA). Theta amplitude and frequency were different between genotypes when similar values of the running speed were considered (data recorded in additional 3 control and 3 mutant mice, see *SI Results* for details). Recordings with silicone probes indicated that the changes in theta rhythm in PV-$\Delta\gamma_2$ mice were not restricted to stratum pyramidale. Depth profiles of theta oscillations were qualitatively similar between genotypes (2 animals per genotype)
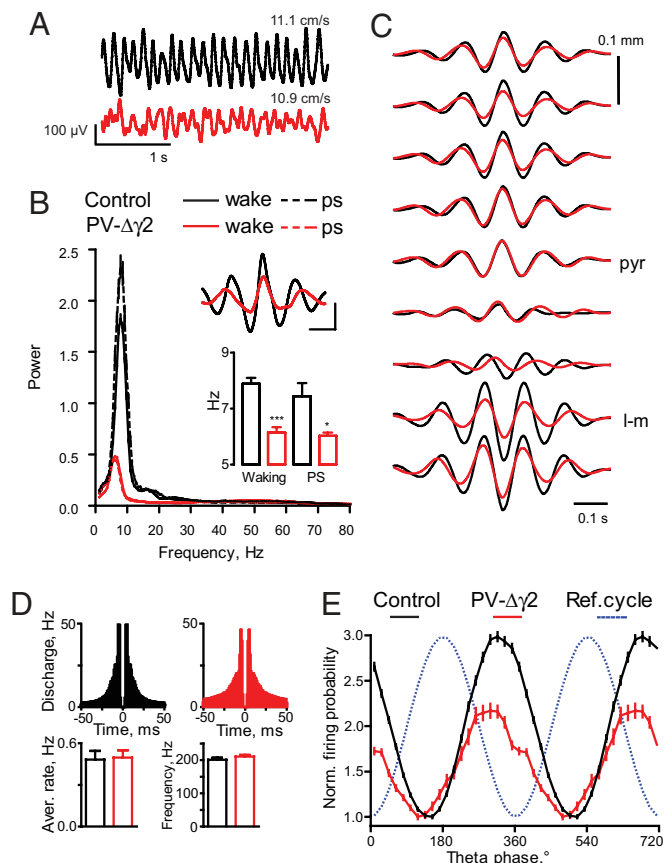
Fig. 2. Theta oscillations are reduced in PV-Δγ2 mice. (*A*) Representative signal examples recorded in CA1 stratum pyramidale during running in control and PVΔγ2 mice (mean running speed is indicated for the 2 epochs). (*B*) Power spectral density of theta oscillations during waking and paradoxical sleep (PS). (*Insets*) Theta peak triggered average of 1–100 Hz bandwidth filtered signal (*Upper*), leading frequency of theta oscillations (*Lower*). (Scale bars: 100 ms, 100 μV) (*C*) Representative averaged depth profiles of theta LFP in CA1 area triggered by theta peaks in stratum pyramidale (pyr) and normalized to their maximal amplitude (5–15 Hz bandwidth). l-m, stratum lacunosum-moleculare. (*D*) Averaged autocorrelograms, average firing rates and burst (>50 Hz) frequency for putative pyramidal cells. (*E*) Modulation of pyramidal cell discharge during theta oscillation. For each group, the discharge probability is normalized by dividing by the minimal value across all bins. *, $P < 0.05$; ***, $P < 0.001$.

(Fig. 2C). Theta phase started to reverse in stratum radiatum and was anti-phase in stratum lacunosum-moleculare and the hippocampal fissure (≈300 to 400 μm below stratum pyramidale). Notably, the amplitude of theta oscillations tended to be lower in strata oriens and lacunosum-moleculare in PV-Δγ2 mice when normalized to the theta amplitude in stratum pyramidale (Fig. 2C), suggesting that theta impairment in PV-Δγ2 mice involves all CA1 layers.

To assess rhythmic organization of neuronal activity during theta oscillations we analyzed theta-phase distribution of neuronal discharge. Because LFP theta did not differ between PS and waking (see above) recordings from both states were pooled. The average firing rates and the fast frequency discharge (exceeding 50 Hz) of putative pyramidal cells did not differ significantly between genotypes (p ≈ 0.4, Fig. 2D). Pyramidal cells, however, fired higher rates during theta epochs in PV-Δγ2 mice than in controls (2.8 ± 0.3 Hz, $n = 56$ cells, in control vs. 3.8 ± 0.4 Hz, $n = 54$ cells, in PV-Δγ2, $P < 0.01$, t test). Pyramidal cells discharged with the maximal probability at the end of the descending portion of the theta cycle in both genotypes (Fig. 2E). The preferred discharge phase of individual pyramidal cells was delayed in PV-Δγ2 mice (36 ± 4° vs. 9 ± 9° before theta trough in control, $n = 45$, and PV-Δγ2, $n = 27$, respectively, $P <$

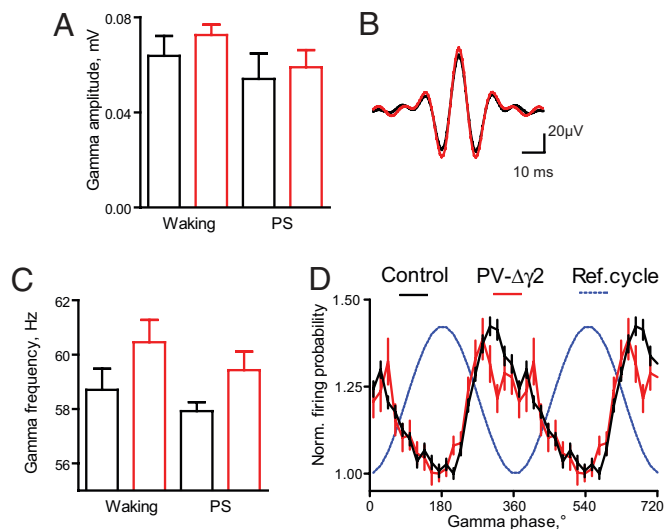**Fig. 3.** Preserved gamma oscillations in PV-Δγ2 mice. (*A*) Amplitude of gamma oscillations during waking and PS (mean ± SEM). (*B*) Gamma peak triggered average of 35–85 Hz bandwidth filtered signal. (*C*) Frequency of gamma oscillations during waking and PS (mean ± SEM). (*D*) Rhythmic modulation of pyramidal cell discharge during theta-associated gamma oscillation. Discharge probabilities are normalized within groups as in Fig. 2*E*.

0.01). Theta rhythm modulated the firing of pyramidal cells in the PV-Δγ2 less than in controls (population modulation coefficients: 0.50, control, vs. 0.37, PV-Δγ2, $P < 0.0001$, paired t test).

Gamma Oscillations Are Intact in Behaving PV-Δγ2 Mice. Fast gamma oscillations (35–85 Hz) were largely unchanged in behaving PV-Δγ2 mice. Integral gamma power and gamma wave amplitude and its variability did not differ between genotypes (p ≈ 0.1, ANOVA, Fig. 3 *A* and *B* and Fig. S5 *A* and *B*). The frequency (computed from interpeak interval) of gamma oscillations tended to be slightly but not significantly elevated in PV-Δγ2 mice ($F_{1,22} = 3.2$, p ≈ 0.09, Fig. 3C). Theta-associated gamma oscillations modulated discharge probability of pyramidal cells in control and PV-Δγ2 mice (Fig. 3D). Pyramidal cells ($n = 26$, control, and $n = 11$, PV-Δγ2) fired the lowest number of spikes near the gamma peaks, whereas maximal firing probabilities were broader distributed between ≈80° before and ≈40° following gamma troughs (not significantly different between genotypes). Pyramidal cells were similarly modulated by gamma oscillations in control and PV-Δγ2 mice (population modulation in pyramidal cells: 0.18 in control, vs. 0.16 in PV-Δγ2, p ≈ 0.2, paired t test).

Coupling of Theta and Gamma Oscillations Is Disrupted in PV-Δγ2 Mice. In control mice gamma oscillations were strongly modulated within the theta cycle with amplitude of gamma oscillation being highest briefly after the peak of the theta cycle (≈20°), as reported in rodents for CA1 stratum pyramidale (6, 8, 38). This coupling between theta and gamma oscillations was severely disrupted in PV-Δγ2 mice (Fig. 4). Amplitude modulation of gamma oscillations was reduced more than 2-fold ($F_{1,22} = 34.5$, $P < 0.0001$, ANOVA, Fig. 4 *B* and *D*). Near theta peaks, gamma amplitude was reduced, whereas, close to theta troughs, it was markedly elevated. Also theta-modulation of gamma oscillation frequency was almost 3-fold lower in PV-Δγ2 mice ($F_{1,22} = 15.5$, $P < 0.001$, ANOVA, Fig. 4 *B* and *D*). The degree of uncoupling was similar during waking and PS (p ≈ 0.1, ANOVA, see also Fig. S6).

To test whether disrupted gamma modulation could simply be caused by the observed alterations in theta rhythm, we analyzed gamma amplitude and frequency distributions, using basic theta oscillation features, such as cycle amplitude, frequency and their normalized variances as explanatory variables (Fig. 4 *C* and *D*).
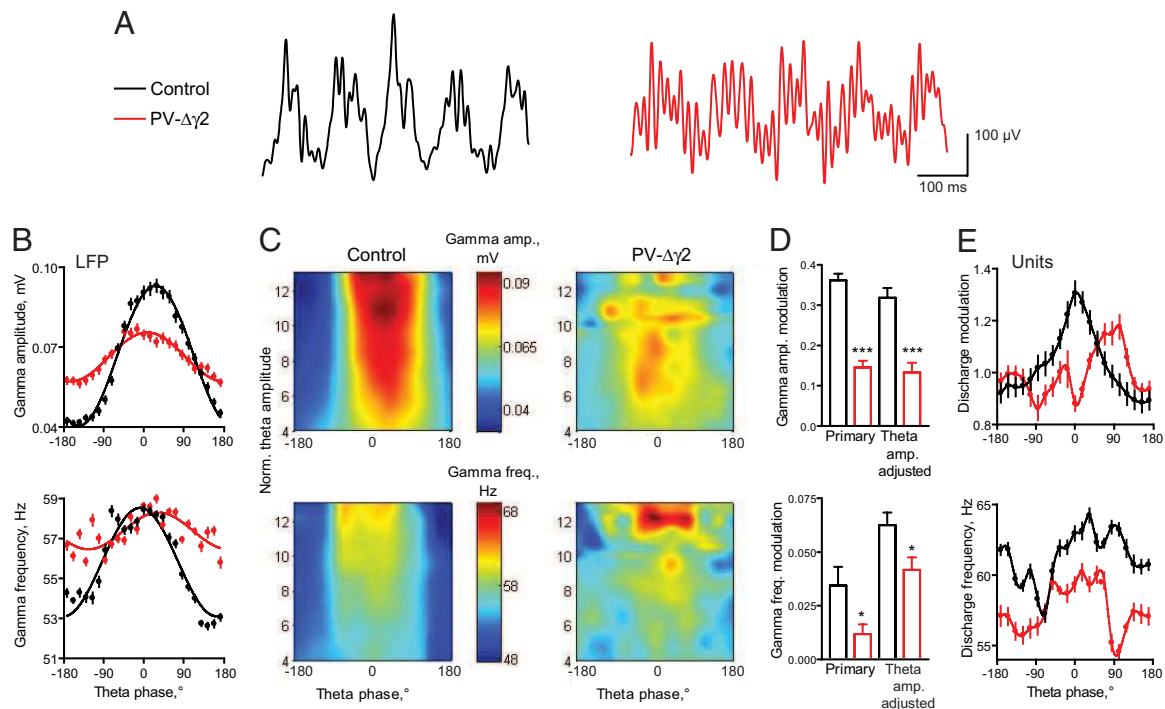
NEUROSCIENCE

Fig. 4. Uncoupling of theta and gamma oscillations. (*A*) Representative signal examples recorded in CA1 stratum pyramidale in control and PV-Δγ₂ mice. (*B*) Altered modulation of gamma amplitude and gamma frequency (mean ± SEM) for all theta oscillation epochs detected during waking (see Fig. S6 for paradoxical sleep statistics). (*C*) Group data showing average modulation of gamma amplitude (upper plots) and frequency (lower plots) for theta cycles of different amplitudes (scaled by the ratio to the delta band activity) during waking. (*D*) Primary (related to plots in *B*) and theta-amplitude adjusted (ANCOVA adjusted mean as shown by the smoothed plots in panel *C*) modulation coefficients. (*E*) Theta-periodicity of the gamma modulation depth (upper plot) and gamma-band discharge frequency (lower plot) in pyramidal cells. *, $P < 0.05$; **, $P < 0.01$; ***, $P < 0.001$.

Strong reduction of gamma modulation in PV-Δγ₂ mice was also evident after adjustment for altered theta rhythm features (at least $P < 0.05$, ANCOVA, see *SI Results* for details). Thus, PV-Δγ₂ mice display two aspects of disrupted coupling between gamma and theta oscillations: first, an overall effect due to attenuated theta rhythm and, second, an effect not directly connected to alteration of theta-features, most likely because of the disruption of the coupling mechanism.

To analyze the modulation of gamma activity during theta on the level of unit activity we first established that higher amplitude gamma cycles better modulate the discharge of concurrently active pyramidal cells ($r = 0.23$, control, $r = 0.13$, PV-Δγ₂, $P < 0.01$). The strength of this association did not differ between genotypes ($z = 1.46$, $p \approx 0.15$). Consistent with the LFP findings, gamma modulation of pyramidal cell ($n = 41$, control, and $n = 39$, PV-Δγ₂) discharge periodically varied in theta cycles in controls but less regularly and weaker in PV-Δγ₂ mice (Fig. 4*E Upper*, individual unit modulation coefficients, 0.24 ± 0.02 in control vs. 0.16 ± 0.02 in PV-Δγ₂, $P < 0.01$, *t* test, see *SI Materials and Methods* for detailed description of the analysis). Therefore, the gamma modulation of spike timing of pyramidal cells as a function of the theta phase is impaired in PV-Δγ₂ mice.

Removal of Synaptic Inhibition onto PV+ Cells in a Hippocampal Network Model Reproduces Experimental Results. To see whether the experimental findings could be accounted for by a theta rhythm generated within the hippocampus we have generated a biophysical CA1 network model. We adopt the same notation used by previous modeling work (21, 22, 39–41) by calling the fast spiking PV+ cells "I cells" (i.e., inhibitory cells) and the pyramidal cells "E cells" (i.e., excitatory cells). For the sake of model generality, we call the hippocampal inhibitory cells that preferentially spike at theta frequency T cells ("theta cells"), and we assume that these cells are not the PV+ interneurons. A recent computational study showed that T cells can generate a coherent population theta rhythm when

they interact with the I cells, i.e., the existence of mutual T → I and I → T connections was shown to be necessary in that model for a coherent theta rhythm on the population level (40). We tested this necessity in a model containing E cells and T and I cells. Fig. 5*Ai* shows the network configuration of E, I and T cells. We represent the E-cell population as a single cell firing at the population frequency; thus this cell produces EPSPs in the I and T cells at gamma frequency, as observed experimentally (42). Fig. 5*A ii–iv* shows a typical result obtained (see also 22). The interplay between the subnetwork consisting of I and T cells is able to produce the theta rhythm, whereas the gamma is generated through a mechanism requiring the E and I cell subnetwork. By means of a model LFP (see *Materials and Methods*), we show that both gamma amplitude and frequency are modulated by the theta phase in this CA1 network model (Fig. 5*C*).

The PV-Δγ₂ network is then simulated by breaking T → I and I → I connections (Fig. 5*B*). Breaking T → I attenuates the theta rhythm (Fig. 5 *B* and *C*) because the T cells are no longer coherent without this connection. The T cells can occasionally generate a theta rhythm, however, this is unstable and less prominent when compared with the control network (Fig. 5*B*). Also, the model PV-Δγ₂ network reproduces the reduction of the theta peak frequency observed experimentally (Fig. 5*C*). The reason for this is that the I cells are prone to spike more without the T cell inhibition and they then provide a greater level of inhibition onto the T cells, diminishing their spike frequency. Also consistent with experimental results, we observed a large reduction in gamma amplitude and frequency modulation by the theta phase in the PV-Δγ₂ network (Fig. 5*C*). Note that the reduction of the gamma modulation by theta is not due only to the reduction of the theta power, because even for the periods when the T cells are able to create a coherent theta rhythm, the lack of T → I connections hinders the modulation of the I cells by the theta.
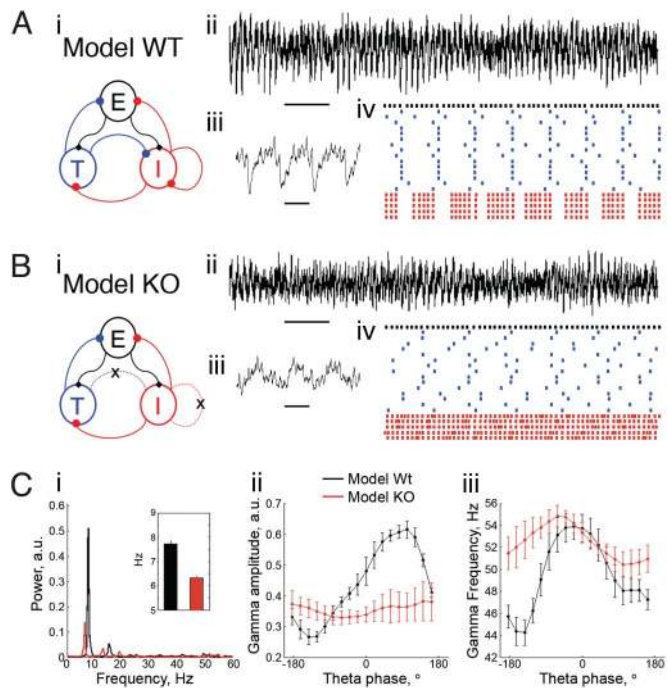
Fig. 5. Lack of inhibition onto I cells reproduces main experimental findings in a simple biophysical CA1 model network. (*A*) (*i*) Network scheme showing the synaptic connections among populations of distinct cell types in the model wild-type (WT). (*ii*) Model LFP from the control network. Ten seconds of simulation are shown (horizontal black bar denotes 1 s); note the existence of a prominent and stable theta rhythm. (*iii*) Model control LFP in shorter time scale showing gamma nesting in the theta rhythm (500 ms of simulation shown; horizontal black bar denotes 100 ms). (*iv*) Representative control network spike rastergram during 1 s of simulation (same color convention for the cells as in *Ai*). Note that the T cells (blue) generate a coherent population theta rhythm and that the spikes of the I cells (red) are modulated by the theta rhythm. The E cell population (black) activity is also shown. (*B*) (*i*) The PV-$\Delta\gamma_2$ network is obtained by removing all of the inhibition onto the I cells (i.e., the T → I and the I → I connections are cut). (*ii*) The theta rhythm becomes unstable and less prominent than the WT network. (*iii*) PV-$\Delta\gamma_2$ LFP trace during a 500 ms period of high theta amplitude shows disrupted coupling of the theta and gamma oscillations. (*iv*) The PV-$\Delta\gamma_2$ spike time rastergram further evidences that the T cells are no longer able to maintain a coherent theta rhythm. (*C*) Group data of 50 simulations with random initial conditions and E cell drive (each parameter set was simulated for 10 s). (*i*) Mean power spectral density showing reduced theta power and slower theta peak frequency (*Inset*) in the PV-$\Delta\gamma_2$ network. (*ii* and *iii*) Averaged modulation of gamma amplitude (*ii*) and frequency (*iii*) by the theta phase showing a reduction of both couplings in the PV-$\Delta\gamma_2$ network. Further details about all of the simulations used in this figure are exposed in *Materials and Methods*.

In summary, the present computational model is consistent with the experimental results; therefore the impairment of an intrahippocampal mechanism of theta generation could be contributing to the alterations in theta and theta-gamma coupling seen in vivo in PV-$\Delta\gamma_2$ mice.

Discussion

In this study we have removed fast GABA$_A$ receptor mediated inhibition from PV+ interneurons. We found that theta oscillations and physiological interactions between gamma and theta rhythms depend on synaptic inhibition onto PV-expressing cells. At the same time, generation of gamma oscillations does not require mutual inhibition between PV+ interneurons.

The MS is critical for the generation of hippocampal theta oscillations (16, 23, 43, 44). The MS provides cholinergic and GABAergic input to the hippocampus. Whereas cholinergic neurons innervate both principal cells and interneurons, GABAergic long-range projection neurons from the MS, which are also PV+, terminate selectively on

hippocampal interneurons, including PV+ BCs (18). Rhythmic inhibition of PV+ hippocampal interneurons by the MS at theta frequency (19, 44) could cause rhythmic IPSPs in principal cells and the corresponding theta dipole in the pyramidal cell layer (16). GABAergic projections from the hippocampus to the MS (45) might contribute to theta rhythm generation in the hippocampus (16, 46). Our data are compatible with the prediction that interneuron-specific ablation of the inhibitory septo-hippocampal projection may severely impair theta rhythm in the hippocampus.

Apart from external sources of rhythmicity, hippocampal networks are prone to synchronize at theta frequency due to intrinsic oscillatory and resonance properties of various neuronal classes. How these classes contribute to theta in behaving animals is more difficult to address; however, hippocampal slices can produce a theta rhythm even when isolated from other brain structures (21, 41, 47). Various studies have investigated how intrahippocampal theta is generated (21, 22, 40–42). Inhibitory interneurons like O-LM and possibly R-LM cells that spike preferentially at theta frequency (T cells) have been reported (21, 41, 42, 48, 49). However, even if cells of a given type spike at theta frequency, this does not imply that they can generate a coherent population theta rhythm, because the cells might be spiking asynchronously. Thus, a mechanism for synchronization of the theta spiking cells is needed. A computational study has shown that T cells can generate a coherent population theta rhythm when they interact with I cells (40). We have explored this mechanism in the context of E, I and T cell networks. Our simulation results showed that this simple CA1 network model can qualitatively reproduce the main experimental findings in the PV-$\Delta\gamma_2$ animals: (*i*) a reduction in theta power; (*ii*) reduction of theta modulation of gamma; (*iii*) a slower theta peak frequency; (*iv*) an instability of the theta rhythm. Based on these results, we hypothesize that impairment of the intrahippocampal mechanism of theta generation, caused by the lack of inhibition onto PV+ cells, contributes to the observed findings.

Hippocampal gamma oscillations are thought to result from interaction of pyramidal cells and interneurons but the role of mutual inhibition between PV+ interneurons has been a matter of debate (2, 9, 20). Our results show that mutual inhibition is dispensable for in vivo gamma oscillations and stress the importance of recurrent excitation and feed-back inhibition (9). In all mammals examined, including humans, gamma oscillations are modulated by concurrent theta rhythm (6–10, 50). This theta-gamma coupling may serve as a general coding scheme that coordinates distributed cortical areas, encodes serial information and working memory, and aids theta phase precession of place cells (5, 10–14, 21). Empirical evidence supports such proposals by showing higher levels of theta-gamma coupling during cognitive demands (10, 14). Here, we show that inhibition onto PV+ interneurons is required for theta-gamma coupling, even after controlling for the level of theta power (Fig. 4). These experimental results can be reproduced by our simple computational model, in which the source of inhibition resides within the hippocampus and is constituted by I cells (putative fast spiking, hence PV+ interneurons) and T cells (inhibitory cells that spike preferentially at theta frequency), and in which the theta rhythm arises from their mutual interaction. Furthermore, by suggesting an impairment of an intrahippocampal mechanism of theta generation in PV-$\Delta\gamma_2$ mice, this model is also consistent with the reduction of theta power observed in all CA1 layers, because interneurons targeting pyramidal cells at distinct levels (e.g., soma, apical dendrites) would present reduced theta coherence. We note, however, that the reduction of hippocampal gamma power modulation by theta phase could also be explained by the lack of theta inputs from an external pacemaker (e.g., from GABAergic septal cells) onto I cells. Also the reduction in theta oscillations could be caused by an impairment of the circuitry in the MS: GABAergic projection neurons in the MS are also PV+ and will thus have lost reciprocal GABAergic inhibition and input from hippocampo-septal projections. It is therefore likely that both extra-

and intra hippocampal factors contribute to the in vivo theta alterations observed in the present study.

Our study provides the first functional evidence in vivo, using cell-type-specific perturbation, for the role of inhibitory control over PV+ interneurons in the generation of theta but not gamma oscillations and in the coupling of hippocampal rhythms across different frequency bands. The extent to which hippocampal oscillations in other frequency bands or network activity in other brain regions rely on fast synaptic inhibition of PV+ cells remains to be established.

Materials and Methods

All procedures involving experimental mice had ethical approval from the Regierungspräsidium Karlsruhe, Germany.

Generation of Mice with a Selective Loss of Synaptic Inhibition onto PV+ Neurons. Mice carrying a conditional allele of the GABA$_A$ receptor γ_2 gene (γ_2I77lox; 35) were crossed with transgenic mice expressing Cre recombinase selectively in parvalbumin-positive cells (PVCre mice; 51). All experiments were performed on mice homozygous for the conditional γ_2 allele and hemizygous for the PVCre transgene (PV-$\Delta\gamma_2$) and PVCre negative littermate controls. For details see *SI Materials and Methods*.

In Situ Hybridization and Immunohistochemistry. In situ hybridization experiments were carried out as described in ref. 36. See *SI Materials and Methods* for oligonucleotide sequences and immunohistochemical procedures.

Whole-Cell Recordings. Whole-cell voltage clamp recordings were made in acute transverse hippocampal slices (300 μm thickness) from brains of adult mice as described in ref. 20. For details see *SI Materials and Methods*.

In Vivo Recordings. Wire electrodes (tetrodes or arrays of single wires) or silicone probes were implanted above the hippocampus and subsequently positioned in the CA1 pyramidal cell layer, using LFP and unitary activity as a reference. Unitary and LFP signals were acquired during sleep and exploratory behavior (see *SI Materials and Methods*).

Computer Modeling. We used single compartment models for the E, I and T cells. All cells were modeled by using the Hodgkin-Huxley formalism. The model CA1 network consisted of 1 E, 5 I, and 15 T cells. A greater number of T cells was used to allow the analysis of their synchrony. Detailed information about the model cells and synapses, the model LFP, and numeric and random aspects of this work can be found in *SI Appendix*. All simulations were carried out using the NEURON simulation program (52).

1. Mann EO, Paulsen O (2007) Role of GABAergic inhibition in hippocampal network oscillations. *Trends Neurosci* 30:343–349.
2. Klausberger T, Somogyi P (2008) Neuronal diversity and temporal dynamics: The unity of hippocampal circuit operations. *Science* 321:53–57.
3. Engel AK, Fries P, Singer W (2001) Dynamic predictions: Oscillations and synchrony in top-down processing. *Nat Rev Neurosci* 2:704–716.
4. Buzsaki G, Draguhn A (2004) Neuronal oscillations in cortical networks. *Science* 304:1926–1929.
5. Jensen O, Colgin LL (2007) Cross-frequency coupling between neuronal oscillations. *Trends Cogn Sci* 11:267–269.
6. Bragin A, et al. (1995) Gamma (40–100 Hz) oscillation in the hippocampus of the behaving rat. *J Neurosci* 15:47–60.
7. Penttonen M, Kamondi A, Acsady L, Buzsaki G (1998) Gamma frequency oscillation in the hippocampus of the rat: Intracellular analysis in vivo. *Eur J Neurosci* 10:718–728.
8. Buzsaki G, et al. (2003) Hippocampal network patterns of activity in the mouse. *Neuroscience* 116:201–211.
9. Csicsvari J, Jamieson B, Wise KD, Buzsaki G (2003) Mechanisms of gamma oscillations in the hippocampus of the behaving rat. *Neuron* 37:311–322.
10. Canolty RT, et al. (2006) High gamma power is phase-locked to theta oscillations in human neocortex. *Science* 313:1626–1628.
11. Lisman J (2005) The theta/gamma discrete phase code occuring during the hippocampal phase precession may be a more general brain coding scheme. *Hippocampus* 15:913–922.
12. Senior TJ, Huxter JR, Allen K, O'Neill J, Csicsvari J (2008) Gamma oscillatory firing reveals distinct populations of pyramidal cells in the CA1 region of the hippocampus. *J Neurosci* 28:2274–2286.
13. Sirota A, et al. (2008) Entrainment of neocortical neurons and gamma oscillations by the hippocampal theta rhythm. *Neuron* 60:683–697.
14. Tort AB, et al. (2008) Dynamic cross-frequency couplings of local field potential oscillations in rat striatum and hippocampus during performance of a T-maze task. *Proc Natl Acad Sci USA* 105:20517–20522.
15. Jones MW, Wilson MA (2005) Theta rhythms coordinate hippocampal-prefrontal interactions in a spatial memory task. *PLoS Biol* 3:e402.
16. Buzsaki G (2002) Theta oscillations in the hippocampus. *Neuron* 33:325–340.
17. Buzsaki G, Eidelberg E (1983) Phase relations of hippocampal projection cells and interneurons to theta activity in the anesthetized rat. *Brain Res* 266:334–339.
18. Freund TF, Antal M (1988) GABA-containing neurons in the septum control inhibitory interneurons in the hippocampus. *Nature* 336:170–173.
19. Toth K, Freund TF, Miles R (1997) Disinhibition of rat hippocampal pyramidal cells by GABAergic afferents from the septum. *J Physiol* 500:463–474.
20. Bartos M, et al. (2002) Fast synaptic inhibition promotes synchronized gamma oscillations in hippocampal interneuron networks. *Proc Natl Acad Sci USA* 99:13222–13227.
21. Gloveli T, et al. (2005) Orthogonal arrangement of rhythm-generating microcircuits in the hippocampus. *Proc Natl Acad Sci USA* 102:13295–13300.
22. Tort AB, Rotstein HG, Dugladze T, Gloveli T, Kopell NJ (2007) On the formation of gamma-coherent cell assemblies by oriens lacunosum-moleculare interneurons in the hippocampus. *Proc Natl Acad Sci USA* 104:13490–13495.
23. Buzsaki G, Leung LW, Vanderwolf CH (1983) Cellular bases of hippocampal EEG in the behaving rat. *Brain Res* 287:139–171.
24. Klausberger T, et al. (2003) Brain-state- and cell-type-specific firing of hippocampal interneurons in vivo. *Nature* 421:844–848.
25. Csicsvari J, Hirase H, Czurko A, Mamiya A, Buzsaki G (1999) Oscillatory coupling of hippocampal pyramidal cells and interneurons in the behaving rat. *J Neurosci* 19:274–287.
26. Henze DA, et al. (2000) Intracellular features predicted by extracellular recordings in the hippocampus in vivo. *J Neurophysiol* 84:390–400.
27. Li XG, Somogyi P, Ylinen A, Buzsaki G (1994) The hippocampal CA3 network: An in vivo intracellular labeling study. *J Comp Neurol* 339:181–208.
28. Sik A, Penttonen M, Ylinen A, Buzsaki G (1995) Hippocampal CA1 interneurons: An in vivo intracellular labeling study. *J Neurosci* 15:6651–6665.
29. Hajos N, et al. (2004) Spike timing of distinct types of GABAergic interneuron during hippocampal gamma oscillations in vitro. *J Neurosci* 24:9127–9137.
30. Katona I, Acsady L, Freund TF (1999) Postsynaptic targets of somatostatin immunoreactive interneurons in the rat hippocampus. *J Neurosci* 88:37–55.
31. Cope DW, et al. (2005) Loss of zolpidem efficacy in the hippocampus of mice with the GABA$_A$ receptor gamma2 F77I point mutation. *Eur J Neurosci* 21:3002–3016.
32. Pawelzik H, Hughes DI, Thomson AM (2003) Modulation of inhibitory autapses and synapses on rat CA1 interneurones by GABA(A) receptor ligands. *J Physiol* 546:701–716.
33. Lorez M, Benke D, Luscher B, Mohler H, Benson JA (2000) Single-channel properties of neuronal GABA$_A$ receptors from mice lacking the gamma 2 subunit. *J Physiol* 527 Pt 1:11–31.
34. Schweizer C, et al. (2003) The gamma 2 subunit of GABA(A) receptors is required for maintenance of receptors at mature synapses. *Mol Cell Neurosci* 24:442–450.
35. Wulff P, et al. (2007) From synapse to behavior: Rapid modulation of defined neuronal types with engineered GABA$_A$ receptors. *Nat Neurosci* 10:923–929.
36. Wisden W, Laurie DJ, Monyer H, Seeburg PH (1992) The distribution of 13 GABA$_A$ receptor subunit mRNAs in the rat brain. I. Telencephalon, diencephalon, mesencephalon. *J Neurosci* 12:1040–1062.
37. Borhegyi Z, Varga V, Szilagyi N, Fabo D, Freund TF (2004) Phase segregation of medial septal GABAergic neurons during hippocampal theta activity. *J Neurosci* 24:8470–8479.
38. Buhl DL, Harris KD, Hormuzdi SG, Monyer H, Buzsaki G (2003) Selective impairment of hippocampal gamma oscillations in connexin-36 knock-out mouse in vivo. *J Neurosci* 23:1013–1018.
39. Borgers C, Epstein S, Kopell NJ (2005) Background gamma rhythmicity and attention in cortical local circuits: A computational study. *Proc Natl Acad Sci USA* 102:7002–7007.
40. Rotstein HG, et al. (2005) Slow and fast inhibition and an H-current interact to create a theta rhythm in a model of CA1 interneuron network. *J Neurophysiol* 94:1509–1518.
41. Dugladze T, et al. (2007) Impaired hippocampal rhythmogenesis in a mouse model of mesial temporal lobe epilepsy. *Proc Natl Acad Sci USA* 104:17530–17535.
42. Gloveli T, et al. (2005) Differential involvement of oriens/pyramidale interneurones in hippocampal network oscillations in vitro. *J Physiol* 562:131–147.
43. Andersen P, Bland HB, Myhrer T, Schwartzkroin PA (1979) Septo-hippocampal pathway necessary for dentate theta production. *Brain Res* 165:13–22.
44. Stewart M, Fox SE (1990) Do septal neurons pace the hippocampal theta rhythm? *Trends Neurosci* 13:163–168.
45. Toth K, Borhegyi Z, Freund TF (1993) Postsynaptic targets of GABAergic hippocampal neurons in the medial septum-diagonal band of broca complex. *J Neurosci* 13:3712–3724.
46. Manseau F, Goutagny R, Danik M, Williams S (2008) The hippocamposeptal pathway generates rhythmic firing of GABAergic neurons in the medial septum and diagonal bands: An investigation using a complete septohippocampal preparation in vitro. *J Neurosci* 28:4096–4107.
47. Traub RD, Whittington MA, Colling SB, Buzsaki G, Jefferys JG (1996) Analysis of gamma rhythms in the rat hippocampus in vitro and in vivo. *J Physiol* 493 (Pt 2):471–484.
48. Chapman CA, Lacaille JC (1999) Cholinergic induction of theta-frequency oscillations in hippocampal inhibitory interneurons and pacing of pyramidal cell firing. *J Neurosci* 19:8637–8645.
49. Bourdeau ML, Morin F, Laurent CE, Azzi M, Lacaille JC (2007) Kv4.3-mediated A-type K+ currents underlie rhythmic activity in hippocampal interneurons. *J Neurosci* 27:1942–1953.
50. Hentschke H, Perkins MG, Pearce RA, Banks MI (2007) Muscarinic blockade weakens interaction of gamma with theta rhythms in mouse hippocampus. *Eur J Neurosci* 26:1642–1656.
51. Fuchs EC, et al. (2007) Recruitment of parvalbumin-positive interneurons determines hippocampal function and associated behavior. *Neuron* 53:591–604.
52. Hines ML, Carnevale NT (1997) The NEURON simulation environment. *Neural Comput* 9:1179–1209.